A single tRNA base pair mediates bacterial tRNA-dependent biosynthesis of asparagine

Marc Bailly, Stamatina Giannouli[1], Mickael Blaise, Constantinos Stathopoulos[1],*, Daniel Kern* and Hubert Dominique Becker

Département 'Machineries traductionnelles', UPR 9002 Architecture et Réactivité de l'ARN, Institut de Biologie Moléculaire et Cellulaire du CNRS, 15, Rue René Descartes, F-67084 Strasbourg Cédex, France and [1]Department of Biochemistry and Biotechnology, University of Thessaly, 26 Ploutonos street, 41221 Larissa, Greece

ABSTRACT

In many prokaryotes and in organelles asparagine and glutamine are formed by a tRNA-dependent amidotransferase (AdT) that catalyzes amidation of aspartate and glutamate, respectively, mischarged on tRNA^{Asn} and tRNA^{Gln}. These pathways supply the deficiency of the organism in asparaginyl- and glutaminyl-tRNA synthtetases and provide the translational machinery with Asn-tRNA^{Asn} and Gln-tRNA^{Gln}. So far, nothing is known about the structural elements that confer to tRNA the role of a specific cofactor in the formation of the cognate amino acid. We show herein, using aspartylated tRNA^{Asn} and tRNA^{Asp} variants, that amidation of Asp acylating tRNA^{Asn} is promoted by the base pair U_1–A_{72} whereas the G_1–C_{72} pair and presence of the supernumerary nucleotide U_{20A} in the D-loop of tRNA^{Asp} prevent amidation. We predict, based on comparison of tRNA^{Gln} and tRNA^{Glu} sequence alignments from bacteria using the AdT-dependent pathway to form Gln-tRNA^{Gln}, that the same combination of nucleotides also rules specific tRNA-dependent formation of Gln. In contrast, we show that the tRNA-dependent conversion of Asp into Asn by archaeal AdT is mainly mediated by nucleotides G_{46} and U_{47} of the variable region. In the light of these results we propose that bacterial and archaeal AdTs use kingdom-specific signals to catalyze the tRNA-dependent formations of Asn and Gln.

INTRODUCTION

Flawless protein synthesis requires a set of perfectly paired aminoacyl-tRNAs (aa-tRNAs). It was *de facto* expected that each organism should possess a full complement of aminoacyl-tRNA synthetases (aaRS) capable of matching each amino acid to its cognate tRNA. More recently it became obvious that direct formation of aa-tRNA by charging preformed amino acids on its cognate tRNA with aaRS is not universally conserved (1). In fact, the vast majority of prokaryotes, including almost all prominent human pathogens, use a two-step alternate route to synthesize the aa-tRNAs carrying the amidated amino acid, asparagine (Asn) and glutamine (Gln) (2–4). This pathway that forms the amidated aa-tRNA by transamidation of an aa-tRNA precursor is catalyzed by a tRNA-dependent amidotransferase (AdT). This enzyme supplies the ribosomes of organisms lacking asparaginyl-tRNA synthetase (AsnRS) and glutaminyl-tRNA synthetase (GlnRS), with asparaginyl-tRNA^{Asn} (Asn-tRNA^{Asn}) and glutaminyl-tRNA^{Gln} (Gln-tRNA^{Gln}). In a first step, the mischarged aspartyl-tRNA^{Asn} (Asp-tRNA^{Asn}) and glutamyl-tRNA^{Gln} (Glu-tRNA^{Gln}) are produced by an aspartyl-tRNA synthetase (AspRS) or a glutamyl-tRNA synthetase (GluRS) of relaxed specificity (3,5). These mischarged aa-tRNA escape protein synthesis since they are not binding to elongation factor Tu (EF-Tu) and therefore are not directed to the ribosomes (3,6). Instead, they are substrates for subsequent transamidation by AdTs, thus forming the correctly paired Asn-tRNA^{Asn} and Gln-tRNA^{Gln} that will serve for decoding Asn and Gln codons on the ribosome. *In vivo*, bacterial AdTs ensure formation of either Asn-tRNA^{Asn} (Asp-AdT) or Gln-tRNA^{Gln} (Glu-AdT) or both aa-tRNAs (Asp/Glu-AdT) depending on the genomic context of the organism. However, *in vitro*, all bacterial AdTs studied so far exhibit dual specificity and do not discriminate between the two mischarged aa-tRNAs species. They form both, Asn-tRNA^{Asn} and Gln-tRNA^{Gln}, using the mischarged Asp-tRNA^{Asn} and Glu-tRNA^{Gln} as substrates. Furthermore, the AdT enzymes exhibit different oligomeric structures in bacteria and archaea. Bacteria solely use a heterotrimeric enzyme (GatCAB) encoded by the *gatC*, *gatA* and *gatB* genes. This enzyme which can amidate both Asp attached to tRNA^{Asn} and Glu to tRNA^{Gln} is also encoded

---

by half of the archaeal genomes known so far. However, all archaea use an additional, archaeal-specific AdT of dimeric structure (GatDE) encoded by the *gatD* and *gatE* genes, which only amidates Glu-tRNA[Gln] (7).

Despite the predominant role they play in prokaryotic translation, until recently only few structural and functional data were available for these enzymes (2,8). A recent report describing the 3D structure of *Pyroccocus abyssi* GatDE AdT partially filled up the lack of structural information available for this family of enzymes (9). However, the architecture of the active site of these enzymes and their mode of recognition of the aa-tRNA substrates still remain elusive and the structure/function relationship of this family of enzymes is poorly understood.

Besides Asn and Gln, two other genetically encoded amino acid, cysteine (Cys) and selenocysteine (Sec) are synthesized via a tRNA-dependent pathway involving modification of an amino acid mischarged onto tRNA. Sec-tRNA[Sec], present in many organisms, is formed by modification of Ser-tRNA[Sec] with selenocysteine synthase (10), whereas in the methanogenic archaea lacking cysteinyl-tRNA synthetase, Cys-tRNA[Cys] is formed by modification of *O*-phosphoseryl-tRNA[Cys] by *O*-phosphoseryl-tRNA:Cys-tRNA synthase (11). It is still unknown how these enzymes bind the mischarged aa-tRNA molecule and, more important, what are the structural elements of the tRNA molecule that ensure accurate recognition and reliable enzymatic transformation of the mischarged amino acid.

We focused our interest on recognition of tRNA by the bacterial GatCAB AdT because of the peculiar properties of this enzyme among the AdT family. In contrast to GatDE, GatCAB AdT is able to transform two different amino acids, yielding two different cognate aa-tRNA pairs. In order to efficiently achieve that goal, the enzyme has to be specific enough in order to discriminate the incorrectly charged Asp-tRNA[Asn] from cognate Asp-tRNA[Asp] and the micharged Glu-tRNA[Gln] from cognate Glu-tRNA[Glu]. The discrimination capacity of this enzyme is of extreme importance since amidation of Asp-tRNA[Asp] into Asn-tRNA[Asp] or of Glu-tRNA[Glu] into Gln-tRNA[Glu] would form aa-tRNA species, that, unlike Asp-tRNA[Asn] or Glu-tRNA[Gln], have been predicted to be efficient EF-Tu binders and therefore would lead to misincorporation of amino acids into proteins (12,13). However, specificity of AdTs should also be relaxed enough to form two correctly paired aa-tRNAs, Asn-tRNA[Asn] and Gln-tRNA[Gln]. The mechanism of aa-tRNA discrimination by AdT has not been explored so far and it is not known whether identical tRNA elements trigger recognition of both Asp-tRNA[Asn] and Glu-tRNA[Gln] or if the two tRNA moieties are recognized through distinct elements. In addition, despite the high degree of sequence similarity between the archaeal and bacterial GatCAB AdTs, the possibility that both enzymes utilize different modes of tRNA recognition cannot be excluded. It would therefore be interesting to verify whether AdTs, like aaRSs, exhibit kingdom-specific tRNA recognition patterns.

To gain insight on how Asp-tRNA[Asn] and Glu-ARNt[Gln] are recognized and are discriminated from correctly charged Asp-tRNA[Asp] and Glu-ARNt[Glu] by GatCAB AdTs we investigated the structural elements distinguishing tRNA[Asn] from tRNA[Asp] and tRNA[Gln] from tRNA[Glu] and which should be the potential determinants of specific amidation of tRNA-bound amino acid. We started our investigation by searching the structural elements of tRNA[Asn] that promote conversion of the bound Asp into Asn by the bacterial GatCAB, and those of tRNA[Asp] preventing this conversion. We chose for this study the partners of the tRNA-dependent pathway of Asn formation from *Neisseria meningitidis*, a human pathogenic bacterium, deprived of AsnRS and thus using the AdT pathway to form Asn-tRNA[Asn] (14). We show that a single base pair, U_1–A_{72} determines amidation of Asp bound to tRNA[Asn] by bacterial AdT whereas the supernumerary U_{20A} in the D-loop prevents amidation of Asp bound to tRNA[Asp]. We extended the investigation to the archaeal system and showed that tRNA-dependent Asn formation is promoted by the length of the variable region. Cross-species trans-amidation experiments together with sequence-based comparison of archaeal and bacterial tRNA[Asp] and tRNA[Asn], indicate that transamidations by bacterial and archaeal GatCAB AdTs involve kingdom-specific tRNA elements. Finally, on the basis of the analysis of the sequences of tRNA[Gln] and tRNA[Glu] from bacteria using AdT to form Gln-tRNA[Gln], we predict that bacterial AdTs use the same tRNA structural elements to catalyze the tRNA-dependent formation of Gln and Asn.

MATERIALS AND METHODS

Materials

TLC cellulose plates (20×20 cm^2) were from Merck, hydroxyapatite CHT20 and UNO-Q6 columns from BIO-RAD, DEAE–cellulose DE-52 from Whatman and Heparine-Ultrogel and Cibacron blue-Sepharose from Pharmacia. L-[^{14}C]Asp (207 mCi/mmol) was from Amersham, Dynazyme *Taq* polymerase from Finnzyme, restriction enzymes and the pCYB1 vector were from NEW ENGLAND Biolabs. Epicurian Coli® BL21-CodonPlus™-RIL competent cells were from Stratagene and *N.meningitidis* C58 genomic DNA from ATCC.

AdT from *N.meningitidis*, *Thermus thermophilus* and *Methanosarcina barkeri*

The AdT from *N.meningitidis* was expressed in the *Escherichia coli* BL21 CodonPlus RIL strain transformed with the pCYB1 vector recombined with the reconstituted, artificial, *gatCAB* operon. The protein was purified from the S100 extract by chromatographies on DEAE–cellulose, Phosphocellulose, Hydroxyapatite, Heparine-Ultrogel, Uno-Q6 and Cibacron blue-Sepharose. Pure enzyme (180 mg) was obtained from 35 g of cells. The pure enzyme was free of traces of *E.coli* asparagine synthetases A and B, since incubation of 10 µM of the protein in a standard amidation mixture containing 50 µM of [^{14}C]Asp did not lead to formation of a detectable amount of [^{14}C]Asn (data not shown). The AdT from *T.thermophilus* was purified as described previously (15). AdT-enriched protein fractions from *M.barkeri* were obtained by chromatography of an S100 extract on DEAE–cellulose and identified by western blot with antibodies directed against *T.thermophilus* AdT. The dialyzed fractions were stored at −20°C in 100 mM Na–HEPES buffer, pH 7.2, containing 5 mM

2-mercaptoethanol, 0.1 mM benzamidine and Na_2EDTA and 50% glycerol.

Wild-type, transcribed and mutated tRNA^{Asp} and tRNA^{Asn} from *N.meningitidis*, *T.thermophilus* and total tRNA from *M.barkeri*

For *in vitro* transcription, wild-type and mutated *N.meningitidis* and *T.thermophilus* tRNA^{Asp} and tRNA^{Asn} genes were cloned under control of the T7 RNA polymerase promoter using the cassette-cloning procedure (16). The species beginning with 5′U were cloned downstream the sequence of a self-cleaving ribozyme (17). Transcription, self-cleavage and purification of the transcripts were performed as described previously (16). The transcripts exhibited 60–100% of accepting capacity. For *in vivo* expression, the *T.thermophilus* tRNA^{Asn} gene was extended with the 5′ GAT triplet and the 3′ AATTCAAA octanucleotide to mimic the genomic context of *E.coli* tRNA^{Asn} gene and cloned into the pKK223 vector (16). The tRNA^{Asn} overexpressed in *E.coli* JM 103 strain was purified, after phenol extraction of the nucleic acids, by chromatographies on DEAE–cellulose, Sepharose 4B, Octyl Sepharose 4B and Hydroxyapatite. Pure tRNA^{Asn} (18 mg) (accepting capacity, 36 nmol/mg) was obtained from 200 g of cells. Unfractionated tRNAs from *M.barkeri* were isolated from nucleic acids extracted by shaking the cell suspension (6 g cells in 6 ml of 50 mM sodium acetate buffer, pH 5.1, containing 1 mM $MgCl_2$ and 10 mM Na_2EDTA) briefly sonicated with 1 vol of acid-buffered phenol overnight at room temperature. DNA and long RNAs were precipitated by addition of 20% isopropanol to the aqueous layer recovered by centrifugation. The tRNAs recovered by DEAE–cellulose chromatography were precipitated with 60% isopropanol and dissolved in water.

Preparation of [^{14}C]Asp-tRNAs

The standard aminoacylation mixture (50–200 µl) containing 100 mM Na–HEPES, pH 7.2, 30 mM KCl, 2 mM ATP, 12 mM $MgCl_2$, 10–100 µM L-[^{14}C]Asp (300 cpm/pmol), 2–10 µM tRNA or transcripts and 0.2–1 µM of *T.thermophilus* non-discriminating AspRS was incubated 10 min at 50°C. The reaction was stopped by acid-buffered phenol and chloroform extractions; the [^{14}C]Asp-tRNA was precipitated with ethanol in the aqueous layer recovered by centrifugation, sedimented, re-dissolved in water and the concentration was determined by scintillation counting of aliquots after TCA precipitation.

tRNA-dependent amidation assays

The standard reaction mixture of 50 µl containing 100 mM Na–HEPES buffer, pH 7.2, 12 mM $MgCl_2$, 2 mM L-Asn, 1 mM ATP, 40–400 pmol [^{14}C]Asp-tRNA and appropriate amounts of *N.meningitidis* or *T.thermophilus* AdT or 5 µl of *M.barkeri* GatCAB enriched fraction was incubated 30 min at 37°C. The kinetic constants were measured in the standard reaction mixture containing 0.8–8 µM [^{14}C]Asp-tRNA and 25 or 250 nM of AdT when K_M or k_{cat}/K_M was measured, respectively. After incubation times ranging from 0 to 240 s, 10 µl aliquots were withdrawn, supplemented with 40 µl of water and mixed with phenol–chloroform

to stop the reaction. When pure AdT was used, the [^{14}C]aa-tRNA present in the aqueous layer recovered by centrifugation, was deacylated by 30 min incubation at 80°C in the presence of 25 mM KOH, followed by neutralization with HCl. When an AdT-enriched *M.barkeri* protein fraction was used the [^{14}C]aa-tRNA was precipitated after phenol–chloroform extraction with ethanol to remove the traces of free Asn that could have been formed by contaminating asparagine synthetases, dissolved in 50 µl of water and deacylated as described above. The hydrolysate was dried in a Speed-Vac, dissolved in 3 µl of water and fractionated by TLC on cellulose plates (20×20 cm^2) extended by a 3MM Whatman paper sheet (20×5 cm^2), with a solvent containing 2-propanol/formic acid/water (80:4:20, by vol). The [^{14}C] amino acids were revealed by scanning the 2 h exposed image plate with a Fuji Bioimager.

The half-lifes of wild-type and mutated [^{14}C]Asp-tRNA^{Asn} (45 min) were determined from deacylation kinetics conducted by TCA precipitation after various incubation times of 10 µl aliquots of the amidation mixtures deprived of AdT followed by scintillation counting. Since the kinetics of [^{14}C]Asp-tRNA^{Asn} amidation were conducted within 4 min, the decrease of the concentration of [^{14}C]Asp-tRNA promoted by deacylation was negligible. However, since [^{14}C]Asn-tRNA^{Asn} is less stable (12 min) the kinetics of formation of [^{14}C]Asn-tRNA^{Asn} were established without precipitation of the aa-tRNA by determining the total, free and tRNA-bound, [^{14}C]Asn.

Quantification of the [^{14}C]Asn

The intensities of the [^{14}C]Asn spots were quantified using the volume rectangle tool of the Quantity One software (BIO-RAD). The intensity units of each spot were corrected by subtraction of the background intensity and converted into pmoles of [^{14}C] amino acids by determining, for each TLC plate, the specific activity (Intensity Units/pmol) of the [^{14}C]aa. This value is an average of at least five determinations and was determined from ratio of the intensity units of the spot over the amount (pmol) of [^{14}C]aa-tRNA present.

RESULTS AND DISCUSSION

Establishment of the kinetic behavior of *N.meningitidis* AdT

The aim of this work was to identify the structural elements of tRNA responsible for specific amidation of Asp acylating tRNA^{Asn} into Asn. This investigation requires synthesis of a series of tRNA^{Asn} mutants and the use of an assay that allows monitoring of the effect of the mutations on the tRNA-dependent Asn synthesis. For this purpose we chose to measure the effect of tRNA mutations on the efficiency on the AdT-catalyzed Asp amidation by establishing the kinetic constants of the aspartylated tRNA variants. However, the amidation assay (Materials and Methods) used to analyze AdT activity has, so far, never been applied to kinetic measurements. The absence of kinetic studies on GatCAB AdTs is mainly due to the instability of the ester bond between amino acid and tRNA of the aa-tRNA substrate which might

not allow accurate kinetic measurements. Moreover, another unsolved question is whether AdTs behave similar to Michaelian enzymes or not. Finally, since establishment of kinetic constants for the various aspartylated tRNA variants requires pure aa-tRNA species, the use of *in vitro* transcribed tRNA species is impossible to circumvent. However, the activity of the GatCAB AdTs studied so far was determined using charged, post-transcriptionally modified tRNA^{Asn} or tRNA^{Gln} species expressed *in vivo*. Thus the influence of the tRNA post-transcriptional modifications on recognition by GatCAB AdT of the tRNA moiety of aa-tRNA remains unknown.

The first part of this study consisted in the set up of the kinetic measurements of the tRNA-dependent formation of Asn by *N.meningitidis* AdT. We purified the enzyme to homogeneity from an *E.coli* overexpressing strain, and verified that it was not contaminated by measurable traces of *E.coli* asparagine synthetases A and B catalyzing tRNA-independent Asn formation (Materials and Methods). Since the tRNA mutational investigation rests on the use of a variety of *in vitro* transcribed tRNAs, we first synthesized a *N.meningitidis* tRNA^{Asn} T7 transcript. The transcript was aspartylated by *T.thermophilus* non-discriminating AspRS to almost 100% (data not shown). Stability of the ester bond of this Asp-tRNA^{Asn} species was checked by incubation in the transamidation mixture that will subsequently be used. In these conditions the half-life of this aa-tRNA was of 45 min at 37°C (Materials and Methods). We then tested the ability of the [^{14}C] aspartylated tRNA^{Asn} transcript to be amidated in a standard reaction mixture. Incubation of 100 pmol of [^{14}C]Asp-tRNA^{Asn} with 10 pmol of *N.meningitidis* AdT during 30 min at 37°C resulted in a full conversion into [^{14}C]Asn-tRNA^{Asn}, confirming that aspartylated tRNA^{Asn} transcript deprived of the post-transcriptional modifications is a suitable substrate for *N.meningitidis* AdT (data not shown).

For kinetic measurements of the transamidation reaction we chose to take time plots ranging from 30 s to 2 min, and confirmed by TCA precipitation of aliquots of the reaction mixture that, in agreement with the half-life of the Asp-tRNA^{Asn}, deacylation of the aa-tRNA within this time scale is negligible. Figure 1A shows the TLC analyzing the conversion of [^{14}C]Asp-tRNA^{Asn} into [^{14}C]Asn-tRNA^{Asn} for a range of aa-tRNA concentrations varying from 0.8 to 8 μM. The initial rates derived from this analysis (Materials and Methods) were used to draw the double reciprocal plot (Figure 1B). The linearity of this plot unambiguously proves that *N.meningitidis* AdT behaves like a Michaelian enzyme. The K_M (1.2 μM) and k_{cat} (0.64 s^{-1}) values of *N.meningitidis* AdT for the cognate aspartylated transcript were determined from two independent measurements. The influence of the post-transcriptional modifications of tRNA on the efficiency of the AdT-catalyzed reaction was analyzed by comparing the kinetic constants of amidation of Asp acylating either *T.thermophilus* tRNA^{Asn}, purified from an *E.coli* expressing strain, or *N.meningitidis* T7 tRNA^{Asn} transcript. Since *N.meningitidis* AdT amidates aspartylated tRNA^{Asn} from *T.thermophilus* (K_M = 0.6 μM, k_{cat} = 0.34 s^{-1}) and *N.meningitidis* (Table 1) with comparable efficiencies, the post-transcriptional modifications of tRNA^{Asn} are of minor importance in transamidation,
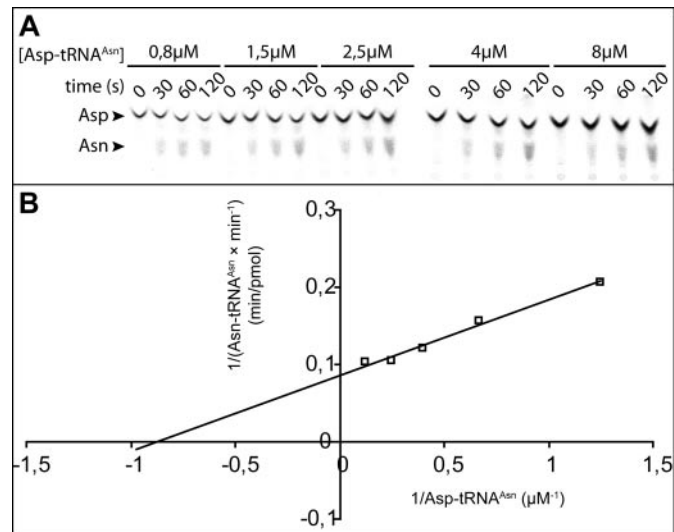

Figure 1. Determination of the kinetic constants of amidation of Asp esterifying the tRNA^{Asn} transcript by *N.meningitidis* AdT. (**A**) Autoradiogram of the TLC plate analysing the conversion of tRNA-bound [^{14}C]Asp into [^{14}C]Asn catalyzed by 25 nM of pure *N.meningitidis* AdT as a function of the concentration [^{14}C]Asp-tRNA^{Asn} (μM) and time (s). The concentrations of aa-tRNA are indicated on the top of each series of time plots. The reactions were conducted as described in Materials and Methods. The remaining [^{14}C]Asp and the [^{14}C]Asn formed in 10 μl aliquots after various time intervals are determined by TLC analysis as described in Materials and Methods. (**B**) Double reciprocal plot: initial rate^{-1} = f ([Asp-tRNA^{Asn}]$^{-1}$). The initial rates were determined from amounts of [^{14}C]Asn formed after increasing incubation times at 37°C shown in (A). The intensities of the spots were quantified as described in Materials and Methods.

justifying the use of variants of tRNA transcripts for characterizing the tRNA transamidation identity elements.

tRNA identity elements for Asp-tRNA^{Asn} transamidation by bacterial AdT

The identification of the candidate nucleotides of tRNA^{Asn} ensuring efficient transamidation of Asp-tRNA^{Asn} into Asn-tRNA^{Asn} was driven by two assumptions. We first assumed that these nucleotides are conserved in the tRNA^{Asn} species of all organisms that use Asp-AdT to form Asn-tRNA^{Asn}, and that the tRNA determinants promoting Asn formation by AdT are not species-specific. This hypothesis is supported by previous results showing that AdTs from various bacterial origins are able to efficiently amidate Asp bound to tRNA^{Asn} from other origins (15,18). The second hypothesis was based on the fact that all AdTs, studied so far, are unable to amidate the other aspartylated tRNA species formed in the cell, namely Asp-tRNA^{Asp}. Therefore, nucleotides conserved in tRNA^{Asn} that can also be found in tRNA^{Asp} should be excluded from set of structural elements potentially responsible for tRNA-dependent Asn formation. We applied these two search criteria on a comparative alignment of 49 bacterial tRNA^{Asn} and tRNA^{Asp} gene sequences. Out of the 8 bp and 9 single nucleotides conserved in all tRNA^{Asn} species only 1 bp, U$_1$–A$_{72}$ in tRNA^{Asn} and G$_1$–C$_{72}$ in tRNA^{Asp}, and 1 nt, U$_{36}$ in tRNA^{Asn} and C$_{36}$ in tRNA^{Asp}, matched our criteria (Figure 2A). In addition, tRNA^{Asp} and tRNA^{Asn} also differ by the length of their D-loop. In tRNA^{Asn}, this loop is

Table 1. Amidation kinetic constants of aspartylated wild-type and mutated tRNA^{Asn} and tRNA^{Asp} transcripts by *N.meningitidis* AdT

Asp-tRNA transcripts Asp-tRNA^X	Kinetic constants K_M (μM)	$\mathcal{L}K_M$	k_{cat} (s^{-1})	$\mathcal{L}k_{cat}$	k_{cat}/K_M (μM^{-1} s^{-1})	$\mathcal{L}k_{cat}/K_M$
Asn wild-type transcript	1.2	1.0	0.64	1.0	0.53	1.0
Asn U$_1$–G$_{72}$	5.6	5.0	0.46	1.4	0.082	6.4
Asn C$_{36}$	0.48	0.4	0.65	1.0	1.35	0.4
Asn + U$_{20A}$	11.93	10.0	0.91	0.7	0.076	7.0
Asn G$_1$–C$_{72}$	n.d.	n.d.	n.d.	n.d.	0.0052	102.0
Asn G$_1$–C$_{72}$,+ U$_{20A}$	n.a.	n.a.	n.a.	n.a.	n.a.	n.a.
Asn G$_1$–C$_{72}$, + U$_{20A}$, C$_{36}$	n.a.	n.a.	n.a.	n.a.	n.a.	n.a.
Asp wild-type	n.a.	n.a.	n.a.	n.a.	n.a.	n.a.
Asp U$_1$–G$_{72}$	n.a.	n.a.	n.a.	n.a.	n.a.	n.a.
Asp ΔU$_{20A}$	n.a.	n.a.	n.a.	n.a.	n.a.	n.a.
Asp U$_1$–G$_{72}$, ΔU$_{20A}$	n.d.	n.d.	n.d.	n.d.	0.0022	241.0
Asp U$_1$–A$_{72}$	n.d.	n.d.	n.d.	n.d.	0.0044	120.0
Asp U$_1$–A$_{72}$, ΔU$_{20A}$	2.7	2.0	0.68	0.9	0.25	2.0
Asp U$_1$–A$_{72}$, ΔU$_{20A}$, U$_{36}$	0.6	0.5	0.46	1.4	0.77	0.7

The tRNA species (X = Asn or Asp) and the mutated nucleotides are indicated. Δ and + indicate the deletion of a nucleotide and the introduction of a supernumerary nucleotide, respectively. Each K_M and k_{cat} value represents the average of at least two independent measurements and their standard deviations were evaluated at 20%; n.a.: not amidated, n.d.: not determined. The losses of affinity (quantified by the increase of K_M, $\mathcal{L}K_M$), of the catalytic rate constant ($\mathcal{L}k_{cat}$) and of the catalytic efficiencies ($\mathcal{L}k_{cat}/K_M$) induced by the mutations are expressed, respectively, by the following ratios: K_M of the Asp-tRNA variant over K_M of wild-type Asp-ARNt^{Asn}, k_{cat} of wild-type Asp-ARNt^{Asn} over k_{cat} of the Asp-tRNA variant and k_{cat}/K_M of wild-type Asp-ARNt^{Asn} over k_{cat}/K_M of the Asp-tRNA variant.

always 1 nt shorter than in tRNA^{Asp} because of the absence of base 20A, which, in tRNA^{Asp}, is mainly a U (Figure 2A). Among these candidates, we defined as transamidation identity elements the nucleotides from tRNA^{Asn} that upon swapping with their tRNA^{Asp} counterparts would significantly decrease the amidation efficiency of the Asp bound to the tRNA^{Asn} variant, whereas transplantation of these elements of tRNA^{Asn} in tRNA^{Asp} should trigger amidation of Asp attached to the tRNA^{Asp} variant.

To validate our approach we first generated a tRNA^{Asn} and a tRNA^{Asp} variant in which all the elements we identified were exchanged by their tRNA^{Asp} and tRNA^{Asn} counterparts, respectively. We thus synthesized the tRNA$^{Asn(G_1-C_{72}, +U_{20A}, C_{36})}$ mutant, in which the U$_1$–A$_{72}$ base pair was mutated into a G$_1$–C$_{72}$ pair, U$_{36}$ was replaced by C$_{36}$ and the D-loop was extended by introduction of a U in position 20A. In the tRNA$^{Asp(U_1-A_{72}, ΔU_{20A}, U_{36})}$ mutant, the G$_1$–C$_{72}$ base pair was mutated into a U$_1$–A$_{72}$ pair, C$_{36}$ was replaced by U$_{36}$ and the D-loop was shortened by deletion of position U$_{20A}$. The two variants were able to be aminoacylated with Asp and they could subsequently be subjected to a transamidation reaction in conditions allowing K_M and k_{cat} measurements (Materials and Methods). The kinetic analysis shows that Asp-tRNA$^{Asn(G_1-C_{72}, +U_{20A}, C_{36})}$ loses completely its capacity to be amidated by *N.meningitidis* AdT whereas Asp-tRNA$^{Asp(U_1-A_{72}, ΔU_{20A}, U_{36})}$ acquires the capability of being amidated as efficiently as the wild-type Asp-tRNA^{Asn} (Figure 3A and Table 1). This result validates the alignment strategy we used to identify the complete set of the potential tRNA transamidation identity elements. To analyze the individual contribution of each element and to characterize the minimal set of elements promoting transamidation we generated T7 transcripts of *N.meningitidis* tRNA^{Asn} variants where the U$_1$–A$_{72}$ base pair and U$_{36}$ were individually exchanged by their corresponding counterparts of *N.meningitidis* tRNA^{Asp} (tRNA$^{Asn(G_1-C_{72})}$ and tRNA$^{Asn(C_{36})}$). To test the influence of the length of D-loop in transamidation of Asp-tRNA^{Asn} we also created a tRNA^{Asn}

mutant in which U$_{20A}$ was introduced in the D-loop (tRNA$^{Asn(+U_{20A})}$) and a tRNA^{Asp} mutant in which U$_{20A}$ was deleted (tRNA$^{Asn(ΔU_{20A})}$). Figure 3A and Table 1 show that tRNA$^{Asn(C_{36})}$ mutant displaying the tRNA^{Asp} anticodon promotes amidation of the bound Asp only two times less efficiently than the wild-type tRNA^{Asn}. This result clearly indicates that the anticodon of the tRNAs we tested does not contribute to the transamidation catalyzed by the GatCAB AdT. Introduction of U$_{20A}$ in the D-loop of tRNA^{Asn} resulted in a loss of transamidation efficiency by almost one order of magnitude as a consequence of a decrease in affinity of the Asp-tRNA$^{Asn(+U_{20A})}$ variant for AdT. Deletion of this nucleotide in the D-loop of tRNA^{Asp} is, however, not sufficient to confer capacity to tRNA^{Asp} to trigger amidation of the bound Asp. Mutation of the first base pair of the acceptor arm of tRNA^{Asn} creates the tRNA$^{Asn(G_1-C_{72})}$ variant whose aspartylated form is still amidated (Figure 3A) but 100-fold less efficiently than Asp-tRNA^{Asn} (Table 1). This loss is mainly attributed to a severely decreased affinity of the aspartylated tRNA^{Asn} variant for AdT. As a consequence, individual kinetic constants could not be measured for this variant, and therefore only the catalytic efficiency was determined (19).

The above-mentioned results strongly suggest that the first base pair of the acceptor arm of tRNA^{Asn} is a major element determining tRNA identity for transamidation by AdT. Indeed, transplantation of this element into tRNA^{Asp} generates the tRNA$^{Asp(U_1-A_{72})}$ mutant whose aspartylated form is amidated. However, Asp-tRNA$^{Asp(U_1-A_{72})}$ still exhibits a loss in catalytic efficiency, of two orders of magnitude, compared to the wild-type Asp-tRNA^{Asn} and Asp-tRNA$^{Asp(U_1-A_{72}, ΔU_{20A}, U_{36})}$. The difference in catalytic efficiencies observed between Asp-tRNA$^{Asp(U_1-A_{72})}$ and Asp-tRNA$^{Asp(U_1-A_{72}, ΔU_{20A}, U_{36})}$ can be attributed to different nucleotides in position 36 or to distinct sizes of the D-loops of the two tRNAs. However, we showed that position 36 of the anticodon does not belong to the identity elements. Further, nucleotide U$_{20A}$ being absent in the D-loop of tRNA^{Asn}
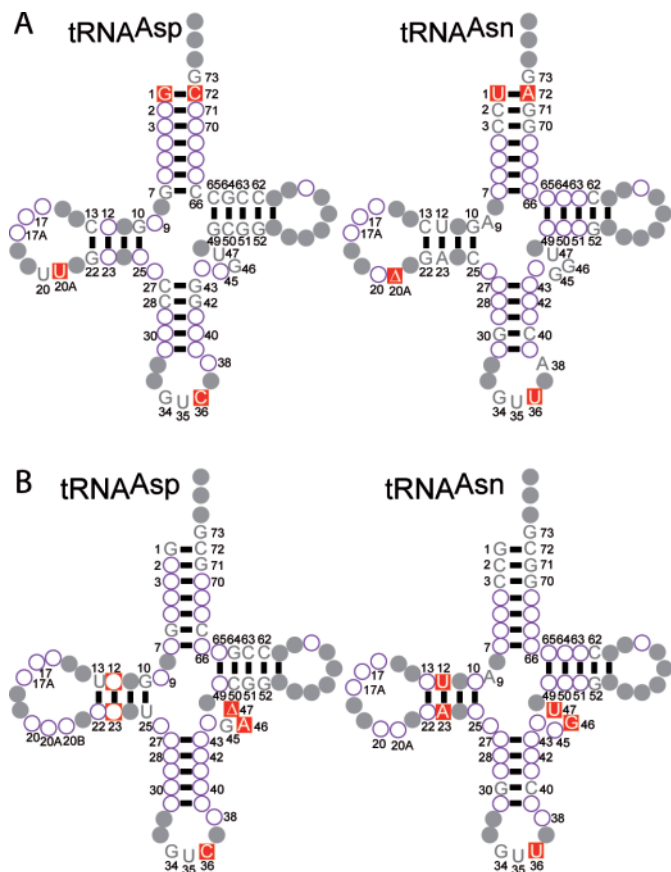
Figure 3. Analysis of the amidation efficiencies of Asp bound to wild-type and mutated tRNA^{Asn} and tRNA^{Asp} by *N.meningitidis* (**A**) and *T.thermophilus* (**B**) AdTs. The reactions were conducted and the samples were treated as described in Materials and Methods. The remaining Asp and the Asn formed after 20 min incubation were analyzed in 10 μl aliquots by TLC after deacylation of the [^{14}C]aa-tRNA. The mutations introduced in the tRNAs are indicated on the top of each lane; Δ and + indicate deletion and insertion of a nucleotide, respectively.

Figure 2. Comparative alignment of tRNA^{Asn} and tRNA^{Asp} sequences from bacteria (**A**) and archaea (**B**) using AdT to form Asn-tRNA^{Asn}. The cloverleaf structures of the consensus sequences of 49 bacterial (A) and 16 archaeal (B) tRNA^{Asp} and tRNA^{Asn} sequences are compared. Grey circles represent nucleotides conserved in all tRNA species. Purple open circles correspond to positions for which the nature of the base varies in the considered tRNA species. Grey nucleotides are conserved in tRNA^{Asp} and tRNA^{Asn}. White nucleotides in red boxes correspond to positions for which the nature of the base is strictly conserved in all tRNA^{Asn} species but differs in all tRNA^{Asp} species. The white triangle in a red box corresponds to the lack of the considered nucleotide in all tRNA^{Asn} species as compared to the tRNA^{Asp} species.

it cannot be considered *per se* as an identity element, and should therefore more likely act as an anti-determinant that decreases recognition of aspartylated tRNA^{Asp}.

To verify this hypothesis we deleted nucleotide U$_{20A}$ from tRNA$^{Asp(U_1-A_{72})}$ and added a U$_{20A}$ in tRNA$^{Asn(G_1-C_{72})}$. As expected, Asp-tRNA$^{Asp(U_1-A_{72}, ΔU_{20A})}$ is transamidated nearly as efficiently as wild-type Asp-tRNA^{Asn} by *N.meningitidis* AdT whereas Asp-tRNA$^{Asn(G_1-C_{72}, +U_{20A})}$ has completely lost its capacity to be amidated (Figure 3A and Table 1). These results clearly show that efficient transamidation of *N.meningitidis* Asp-tRNAs by the cognate AdT is promoted by a single identity element which is the first base pair of tRNA^{Asn} acceptor arm. Moreover, it shows that amidation of Asp-tRNA^{Asp} is prevented by the presence of the supernumerary nucleotide U$_{20A}$ in the D-loop of tRNA^{Asp} which acts as an anti-determinant. By preventing amidation of Asp bound to tRNA^{Asp}, this position improves specific amidation of Asp bound to tRNA^{Asn}.

To verify if the nucleotides in tRNA^{Asn} determining amidation of the bound Asp in *N.meningitidis*, are conserved
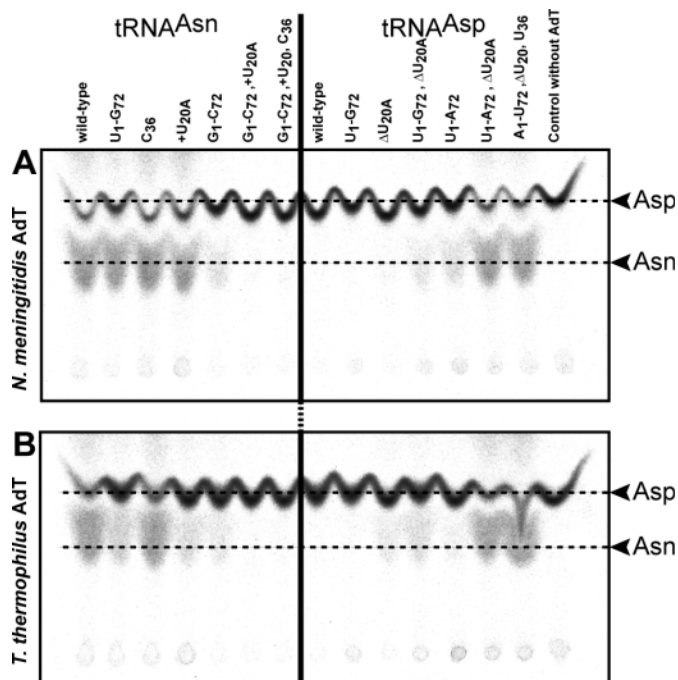
in other bacterial species forming Asn by the tRNA-dependent pathway, we analyzed the amidation profile of Asp bound to the various *N.meningitidis* tRNA^{Asn} and tRNA^{Asp} variants by AdT from a species phylogenetically distant from *N.meningitidis*, like *T.thermophilus*. Figure 3B shows that amidation by *T.thermophilus* AdT requires the same elements of tRNA^{Asn} as the enzyme from *N.meningitidis*. The minor differences observed concern the relative contribution of each element to the amidation efficiency. For the *T.thermophilus* AdT the importance of A$_{72}$ seems increased since Asp-tRNA$^{Asn(U_1-G_{72})}$ is less well amidated by the *T.thermophilus* enzyme than by the *N.meningitidis* one. Additionally, the supernumerary U$_{20A}$ of tRNA^{Asp} is a stronger anti-determinant when amidation is catalyzed by *T.thermophilus* AdT than by the *N.meningitidis* enzyme. These conclusions are supported by the following observations: (i) Asp-tRNA$^{Asn(+U_{20A})}$ is less well amidated by AdT from *T.thermophilus* than by that from *N.meningitidis*, (ii) Asp-tRNA$^{Asn(Δ_{20A})}$ is slightly amidated by *T.thermophilus* AdT but not by that of *N.meningitidis* and (iii) when deprived of U$_{20A}$, amidation efficiency of Asp-tRNA$^{Asp(U_1-A_{72})}$ increases more with *T.thermophilus* AdT than with the *N.meningitidis* one (Figure 3A and B). However, since the same positions of tRNA^{Asn} and of tRNA^{Asp}, respectively, promote and prevent transamidation by the AdTs from *T.thermophilus* and from *N.meningitidis* both enzymes discriminate Asp-tRNA^{Asn} from Asp-tRNA^{Asp} by similar mechanisms. So far among aa-tRNA forming enzymes, only alanyl-tRNA synthetase has been shown to
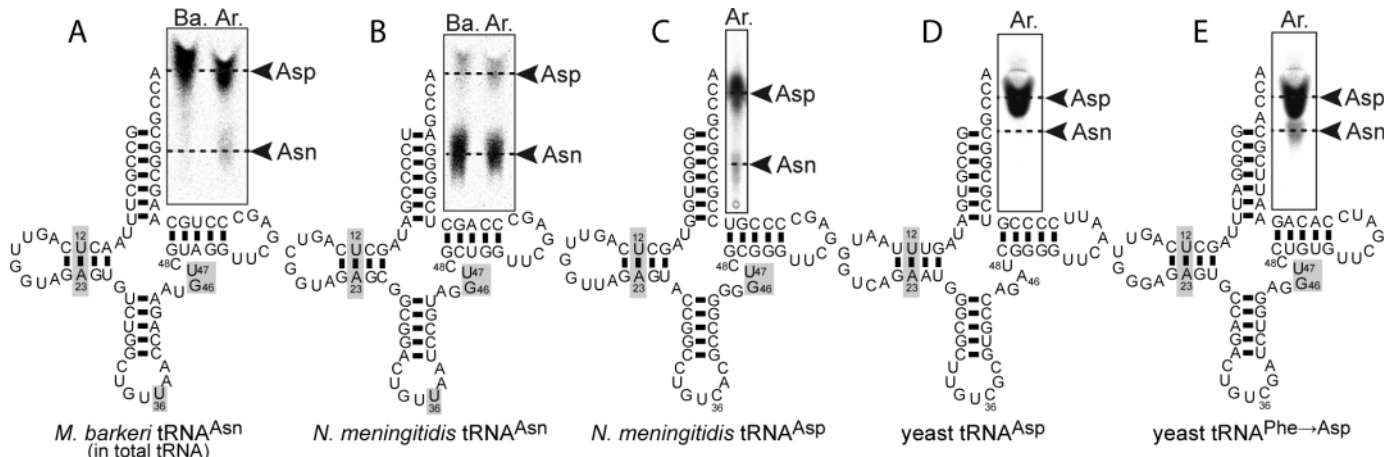
Figure 4. (A–E) Identification of the archaeal tRNA^{Asn} transamidation identity elements by cross-species transamidation experiments. The transamidation mixture containing 2 μM aspartylated *N.meningitidis* tRNA^{Asp} or tRNA^{Asn} or aspartylated yeast tRNA^{Asp} or tRNA$^{Phe \rightarrow Asp}$ or aspartylated tRNA^{Asn} in unfractionated *M.barkeri* tRNA and either 25 nM *N.meningitidis* AdT (Ba.) or 5 μl of *M.barkeri* AdT-enriched fraction (Ar.) was incubated during 60 min at 37°C. The remaining Asp and the Asn formed are determined after deacylation of the [^{14}C]aa-tRNA by TLC analysis as described in Materials and Methods. The inset shows the spots of [^{14}C]Asp and [^{14}C]Asn after scanning of the image plate. The cloverleaf structures of the tRNAs used in these experiments are displayed. In each tRNA species the nucleotides belonging to the archaeal set of transamidation identity determinants predicted by comparative sequence alignment (Figure 2B) are in grey boxes.

display a tRNA identity set constituted only by a single base pair (20).

Finally we wondered whether the tRNA^{Asn} elements we identified as being responsible for amidation of the bound Asp, could be brought down to the single U$_1$ base. For this reason, we constructed the tRNA$^{Asn(U_1 \text{-} G_{72})}$ and tRNA$^{Asp(U_1 \text{-} G_{72}, \Delta U_{20A})}$ variants and analyzed their ability to trigger amidation of the bound Asp by AdT. Figure 3 and Table 1 show that Asp-tRNA$^{Asn(U_1 \text{-} G_{72})}$ is transamidated only 6.4 times less efficiently than the wild-type Asp-tRNA^{Asn}, but 16 times more efficiently than Asp-tRNA$^{Asn(G_1 \text{-} C_{72})}$. This result suggests that U$_1$ from acceptor arm is the major identity determinant for amidation and that A$_{72}$ might be dispensable. Similarly, introduction of U$_1$–G$_{72}$ in tRNA$^{Asp(\Delta U_{20A})}$ confers competency to tRNA^{Asp} to promote amidation of the acylating Asp by AdT. However, the tRNA$^{Asp(U_1 \text{-} G_{72}; \Delta U_{20A})}$ variant promotes amidation of the bound Asp 120-fold less efficiently than the tRNA$^{Asp(U_1 \text{-} A_{72}, \Delta U_{20A})}$ variant. This indicates that nucleotide A$_{72}$ contributes more efficiently to amidation of Asp by AdT in the framework of tRNA^{Asp} than in that of tRNA^{Asn}.

Kingdom-specific tRNA elements for tRNA-dependent asparagine formation

Besides bacteria, almost half of the archaea use also a GatCAB AdT to form Asn-tRNA^{Asn} (7,21). The archaeal GatC, GatA and GatB subunits share a high degree of sequence homology with their bacterial counterparts and both AdTs display the same functional properties since they transamidate *in vitro* both Asp-tRNA^{Asn} and Glu-tRNA^{Gln} (7). However, the tRNA elements promoting transamidation differ for the two phylae. In archaea, the first base pair of tRNA^{Asn}, a G$_1$–C$_{72}$ pair, is also present in tRNA^{Asp} (Figure 2B), indicating that, in contrast to bacteria, this base pair cannot specifically promote transamidation of Asp-tRNA^{Asn}.

Applying the strategy of comparative tRNA alignments to the archaeal tRNA^{Asp} and tRNA^{Asn} species, we identified the U$_{12}$–A$_{23}$ base pair from the D-stem, nucleotide U$_{36}$ and nucleotides G$_{46}$ and U$_{47}$ from the V-region of tRNA^{Asn} as the potential identity elements promoting tRNA-dependent transamidation by the archaeal AdT (Figure 2B). These nucleotides differ in archaeal tRNA^{Asp} where the 12–23 bp is mainly G–C, C is found in position 36 and the V-region is 1 nt shorter than in tRNA^{Asn} because nt 47 is missing whereas A is found in position 46 (Figure 2B). Interestingly, the elements that could determine amidation of Asp bound to archaeal tRNA^{Asn} are conserved in all bacterial tRNA^{Asn} (Figure 2A). Moreover, nucleotides G$_{46}$ and U$_{47}$ of the V-region are also conserved in all bacterial tRNA^{Asp} (Figure 2A), which mostly, like *N.meningitidis* tRNA^{Asp}, also display the U$_{12}$–A$_{23}$ base pair. These observations indicate that the archaeal AdT should not be able to discriminate aspartylated bacterial tRNA^{Asn} and tRNA^{Asp}. However, since all archaeal tRNA^{Asn} possess the G$_1$–C$_{72}$ base pair shown to prevent amidation by bacterial AdT, one can predict that aspartylated archaeal tRNA^{Asn} should not be a suitable substrate for bacterial AdT.

To verify these predictions, we performed cross-species transamidation experiments. tRNA^{Asn} from *M.barkeri* is aspartylated by *T.thermophilus* non-discriminating AspRS and the esterifying Asp is amidated by AdT from *M.barkeri* (Figure 4A). However, as expected, *N.meningitidis* AdT is unable to promote amidation of Asp bound to the archaeal tRNA^{Asn} (Figure 4A), whereas AdT from *M.barkeri* amidates Asp bound to both tRNA^{Asn} and tRNA^{Asp} from *N.meningitidis* (Figure 4B and C). These results confirm that the tRNA elements determining conversion of the esterifying Asp into Asn differ in the bacterial and archaeal systems. They also show that nt 36, C in tRNA^{Asp} and U in tRNA^{Asn} does not constitute a transamidation identity element in the archaeal system.

To establish that nucleotides G_{46} and U_{47} of the V-region of tRNA^{Asn} are involved in the archaeal transamidation, we performed cross-species reactions using archaeal AdT and transcripts of yeast tRNA^{Asp} and of the yeast tRNA^{Phe} variant (tRNA$^{Phe \rightarrow Asp}$) containing the aspartate aminoacylation identity elements, both efficiently aspartylated by yeast AspRS (16). Both tRNAs contain the U_{12}–A_{23} base pair in the D-stem, but while yeast tRNA^{Asp} displays the V-region of archaeal tRNA^{Asp} (absence of position 47 and A_{46}), the tRNA$^{Phe \rightarrow Asp}$ V-region resembles that of archaeal tRNA^{Asn} (G_{46} U_{47}, Figure 4). As a consequence, these tRNAs are suitable substrates for analyzing the role of the V-region in transamidation by the archaeal AdT. Figure 4D and E shows that the archaeal AdT amidates Asp bound to yeast tRNA$^{Phe \rightarrow Asp}$ but not when bound to yeast tRNA^{Asp}, confirming that transamidation by archaeal AdT is promoted by nucleotides G_{46} and U_{47} of the V-region. This agrees with the incapacity of archaeal AdT to amidate Asp bound to yeast tRNA^{Asp} containing the U_{12}–A_{23} pair. Thus this base pair, like U_{36}, does not constitute a determinant for archaeal transamidation.

However, these results do not allow to conclude whether the identity is determined by the length of the V-region or by the nature of nt 46 and 47; nor they allow to conclude whether these positions are identity elements *per se* or not, because of the critical role they play in the folding of tRNA and in the stability of the L-shaped structure. Nt 46 interacts via three H-bonds with the 13–22 bp of the D-stem, and it has been shown that lack of nt 47 alters the stability of tRNA (22). Therefore discrimination by archaeal AdT between Asp-tRNA^{Asn} and Asp-tRNA^{Asp} could be based on the distinct 3D structures that both tRNAs adopt. Comparison of the tRNA sequences of archaea that use the tRNA-dependent pathway to form Asn shows that, in each species, 9–25 tRNAs contain G_{46} and U_{47} in the V-region. Therefore, selection of Asp-tRNA^{Asn} by the archaeal AdT is likely achieved by the Asp moiety. These observations suggest that the Asp moiety contributes more to recognition of Asp-tRNA^{Asn} by archaeal AdT than by the bacterial homolog where tRNA^{Asn} and tRNA^{Gln} are the unique tRNAs, among all species, to display the elements determining amidation.

Predicting what are the identity elements for amidation of Glu bound to tRNA^{Gln}

Independently of the activity they carry out *in vivo* (Asp- or/ and Glu-AdT), all bacterial AdTs studied so far exhibit *in vitro* dual specificity and form both Asn-tRNA^{Asn} and Gln-tRNA^{Gln}. One of the questions raised by the functional property of AdT is whether tRNA^{Asn} and tRNA^{Gln} display the same set of recognition elements for amidation of the bound amino acids or if AdTs recognize distinct elements of the two tRNA species.

To gain insight into the elements of tRNA^{Gln} promoting amidation of the bound Glu and those of tRNA^{Glu} preventing the amidation we aligned several tRNA^{Gln} and tRNA^{Glu} sequences from bacteria using the transamidation pathway to form Gln-tRNA^{Gln}. The comparative alignment shows that the elements conserved in tRNA^{Gln} but which differ in tRNA^{Glu} are those, which in tRNA^{Asn}, promote conversion of bound Asp into Asn, and those, which in tRNA^{Asp}, prevent
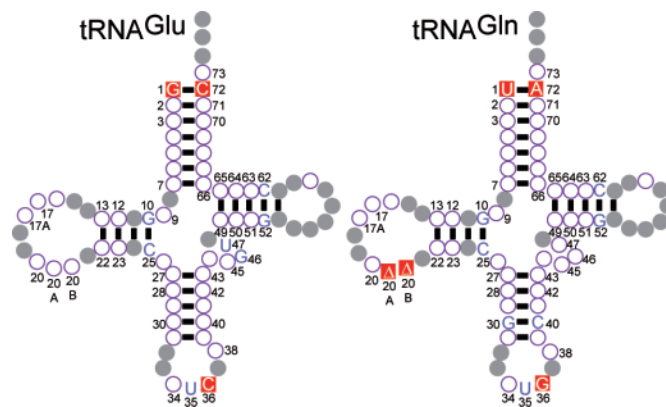

Figure 5. Comparative alignment of tRNA^{Gln} and tRNA^{Glu} sequences from bacteria using AdT to form Gln-tRNA^{Gln}. The cloverleaf structures of the consensus sequences of 101 bacterial tRNA^{Glu} and tRNA^{Gln} sequences are compared. Grey circles represent nucleotides conserved in all tRNA species. Purple open circles correspond to positions for which the nature of the base varies in the considered tRNA species. Blue nucleotides are conserved in tRNA^{Glu} and tRNA^{Gln}. White nucleotides in red boxes correspond to nucleotides strictly conserved in all tRNA^{Gln} species but which differ in all tRNA^{Glu} species. White triangle in red boxes correspond to the lack of a given nucleotide in all tRN^{Gln} species as compared to the tRNA^{Glu} species.

this conversion (Figure 5). This set of elements is constituted by the first base pair of the tRNA acceptor arm, a U_1–A_{72} pair present in tRNA^{Gln} and in tRNA^{Asn} which is substituted in tRNA^{Glu}, like as in tRNA^{Asp} by the G_1–C_{72} pair. In addition like tRNA^{Asp} when compared to tRNA^{Asn}, tRNA^{Glu} displays a supernumerary nucleotide in positions 20A or 20B of the D-loop when compared to tRNA^{Gln} (Figure 5). Similar to tRNA^{Asn} and tRNA^{Asp}, both tRNA^{Gln} and tRNA^{Glu} differ by the 3′ nucleotide of the anticodon, G_{36} in tRNA^{Gln} and C_{36} in tRNA^{Glu}. However, since this nucleotide does not significantly contribute to amidation of Asp bound to tRNA^{Asn}, we can predict that AdTs do not discriminate tRNA^{Gln} from tRNA^{Glu} on the basis of this nucleotide. These results suggest that the same structural elements of AdT are involved in selection of both Asp-tRNA^{Asn} and Glu-tRNA^{Gln}. Further support of this prediction is brought by the following facts: (i) in bacteria that use both Asp-AdT and Glu-AdT activities, tRNA^{Asn} and tRNA^{Gln} contain a U_1–A_{72} base pair while tRNA^{Asp} and tRNA^{Glu} contain a G_1–C_{72} pair and an extended D-loop (Table 2); (ii) in bacteria utilizing only the Asp- or the Glu-AdT activity, the tRNA that promotes the amidation of the bound amino acids, always contains the elements conferring transamidation identity (Table 2); (iii) in bacteria deprived of the AdT, the tRNA^{Asn} and tRNA^{Gln} are directly charged by the cognate aaRS and do not contain these elements.

Confirming experimentally our prediction of the bacterial tRNA^{Gln} transamidation identity set will be difficult to perform since unmodified tRNA^{Glu}, derived by *in vitro* transcription, have been shown to be poor substrates for all bacterial GluRSs studied so far whether they are discriminating or not. In the case of *E.coli* GluRS, it has been shown that the cognate tRNA^{Glu} T7 transcript exhibits a 100-fold reduction in its catalytic efficiency compared to that of tRNA^{Glu} prepared from an overproducing strain (23,24). Thus, confirmation of the predicted bacterial tRNA^{Gln} identity set cannot be conducted with the kinetic approach which rests on the

Table 2. Comparative analysis of the nature of the first base pair and of the D-loop lengths of bacterial tRNA^Asn, tRNA^Asp, tRNA^Gln and tRNA^Glu

Organism	tRNA^Asn 1–72	Dl	tRNA^Asp 1–72	Dl	tRNA^Gln 1–72	Dl	tRNA^Glu 1–72	Dl	AdT Asp	Glu
C.trachomatis	U–A	7	G–C	9 (U20A)	U–A	7	G–C	11 (CC20AB)	+	+
M.tuberculosis	U–A	8	G–C	9 (U20A)	U–A	8	G–C	9 (CU20AB)	+	+
H.pylori	U–A	7	G–C	9 (U20A)	U–A	7	G–C	9 (CA20AB)	+	+
C.jejuni	U–A	7	G–C	9 (U20A)	U–A	7	G–C	8 (U20A)	+	+
C.crescentus	U–A	7	G–C	9 (U20A)	U–A	7	G–C	8 (U20A)	+	+
T.maritima	U–A	8	G–C	10 (U20A)	U–A	7	G–C	8 (C20A)	+	+
A.aeolicus	U–A	8	G–C	10 (C20A)	U–A	8	G–C	11 (CU20AB)	+	+
C.acetobutylicum	U–A	7	G–C	9 (U20A)	U–A	7	G–C	8 (U20A)	+	+
R.prowazekii	U–A	7	G–C	9 (U20A)	U–A	7	G–C	8 (U20A)	+	+
B.melitensis	U–A	7	G–C	9 (U20A)	U–A	7	G–C	8 (U20A)	+	+
M.loti	U–A	7	G–C	9 (U20A)	U–A	7	G–C	8 (U20A)	+	+
A.tumefaciens	U–A	7	G–C	9 (U20A)	U–A	7	G–C	8 (U20A)	+	+
Si.meliloti	U–A	7	G–C	9 (U20A)	U–A	7	G–C	8 (U20A)	+	+
C.tepidum	U–A	7	G–C	10 (U20A)	U–A	7	G–C	8 (U20A)	+	+
C.glutamicum	U–A	8	G–C	9 (U20A)	U–A	8	G–C	9 (CU20AB)	+	+
T.tengcongensis	U–A	7	G–C	9 (U20A)	U–A	7	G–C	8 (U20A)	+	+
B.longum	U–A	8	G–C	9 (U20A)	U–A	7	G–C	8 (U20A)	+	+
B.suis	U–A	7	G–C	9 (U20A)	U–A	7	G–C	8 (U20A)	+	+
T.whipplei	U–A	8	G–C	9 (U20A)	U–A	7	G–C	9 (CU20AB)	+	+
C.burnetii	U–A	8	G–C	9 (U20A)	U–A	7	G–C	9 (CU20AB)	+	+
S.coelicolor	U–A	8	G–C	10 (G20A)	U–A	7	G–C	9 (CU20AB)	+	+
N.meningitidis	U–A	8	G–C	9 (U20A)	U–A	8	G–C	8 (U20A)	+	−
D.radiodurans	U–A	7	G–C	8 (U20A)	A–U	7	G–C	8 (U20A)	+	−
P.aeruginosa	U–A	8	G–C	9 (U20A)	A–U	7	G–C	9 (CU20AB)	+	−
C.perfringens	U–A	7	G–C	9 (U20A)	U–A	7	G–C	8 (U20A)	+	−
R.solanacearum	U–A	8	G–C	9 (U20A)	A–U	9	G–C	9 (CU20AB)	+	−
B.japonicum	U–A	7	G–C	9 (U20A)	U–A	7	G–C	8 (U20A)	+	−
Pirellula sp.	U–A	7	G–C	9 (U20A)	U–A	8	G–C	9 (CU20AB)	+	−
N.europaea	U–A	8	G–C	9 (U20A)	U–A	7	G–C	9 (CU20AB)	+	−
P.syringae	U–A	8	G–C	9 (U20A)	A–U	7	G–C	9 (CU20AB)	+	−
B.subtilis	U–A	7	G–C	9 (U20A)	U–A	7	G–C	8 (U20A)	−	+
S.aureus	U–A	7	G–C	8 (U20A)	U–A	7	G–C	8 (U20A)	−	+
U.urealyticum	G–C	7	G–C	8 (U20A)	U–A	7	G–C	9 (UG20AB)	−	+
B.burgdorferi	U–A	7	G–C	9 (U20A)	U–A	7	G–C	8 (U20A)	−	+
M.genitalium	G–C	7	G–C	8	U–A	7	G–C	9 (UU20AB)	−	+
T.pallidum	U–A	8	G–C	9 (U20A)	U–A	7	G–C	8 (U20A)	−	+
Synechocystis sp.	U–A	7	G–C	9 (U20A)	U–A	7	G–C	9 (CU20AB)	−	+
L.monocytogenes	U–A	8	G–C	8 (U20A)	U–A	7	G–C	8 (U20A)	−	+
S.pyogenes	U–A	9	G–C	8 (U20A)	U–A	7	G–C	8 (U20A)	−	+
Nostoc sp.	C–U	7	G–C	9 (U20A)	U–A	10	G–C	9 (CU20AB)	−	+
M.pulmonis	G–C	7	G–C	9 (U20A)	U–A	7	G–C	8 (U20A)	−	+
F.nucleatum	G–C	8	G–C	9 (U20A)	U–A	7	G–C	8 (U20A)	−	+
S.agalactiae	U–A	9	G–C	8 (U20A)	U–A	7	G–C	8 (U20A)	−	+
T.elongatus	U–A	7	G–C	9 (U20A)	U–A	7	G–C	9 (CU20AB)	−	+
L.interrogans	U–A	8	G–C	9 (U20A)	U–A	7	G–C	8 (U20A)	−	+
O.iheyensis	U–A	7	G–C	9 (U20A)	U–A	7	G–C	8 (U20A)	−	+
S.mutans	U–A	9	G–C	8 (U20A)	U–A	7	G–C	8 (U20A)	−	+
B.halodurans	U–A	7	G–C	9 (U20A)	U–A		G–C	8 (U20A)	−	+
C.tetani	U–A	7	G–C	10 (U20A)	U–A	7	G–C	8 (U20A)	−	+
E.faecalis	U–A	9	G–C	9 (U20A)	U–A	7	G–C	8 (U20A)	−	+
L.plantarum	G–C	8	G–C	10 (U20A)	U–A	7	G–C	9 (UU20AB)	−	+
B.anthracis	U–A	7	G–C	8 (U20A)	U–A	7	G–C	8 (U20A)	−	+
B.aphidicola	U–A	8	G–C	9 (U20A)	U–A	8	G–C	8 (U20A)	−	−
V.cholerae	U–A	8	G–C	9 (U20A)	A–U	7	G–C	9 (CU20AB)	−	−
E.coli	U–A	8	G–C	9 (U20A)	U–A	7	G–C	9 (CU20AB)	−	−
H.influenzae	U–A	8	G–C	9 (U20A)	U–A	7	G–C	9 (CU20AB)	−	−
P.multocida	U–A	8	G–C	9 (U20A)	U–A	7	G–C	9 (CU20AB)	−	−
Y.pestis	U–A	8	G–C	9 (U20A)	U–A	7	G–C	9 (CU20AB)	−	−
S.typhimurium	U–A	8	G–C	9 (U20A)	U–A	7	G–C	9 (CC20AB)	−	−
X.campestris	G–C	9	G–C	9 (U20A)	U–A	7	G–C	9 (CU20AB)	−	−
X.axonopodis	G–C	9	G–C	9 (U20A)	U–A	7	G–C	9 (CU20AB)	−	−
S.oneidensis	U–A	8	G–C	9 (U20A)	U–A	7	G–C	9 (CU20AB)	−	−
S.flexneri 2a	U–A	8	G–C	9 (U20A)	U–A	7	G–C	9 (CC20AB)	−	−
X.fastidiosa	G–C	9	G–C	9 (U20A)	U–A	7	G–C	9 (CU20AB)	−	−
S.enterica	U–A	8	G–C	9 (U20A)	U–A	7	G–C	9 (CC20AB)	−	−
B.thetaiotaomicron	U–A	9	G–C	9 (U20A)	U–A	7	G–C	8 (U20A)	−	−

The nature of the first base pair (1–72) and the number of nucleotides of the D-loop (DI) in the four tRNAs are indicated for a sampling of 67 bacterial species. When present, the nature of nucleotides 20A and/or 20B is indicated into brackets; + and − indicate whether AdT is or is not involved in formation of Asn-tRNA^Asn (Asp) or Gln-tRNA^Gln (Glu), respectively. The shaded cells indicate conservation of the U_1–A_72 bp in tRNA^Asn and tRNA^Gln and the *in vivo* activity of the AdT: Asp- or Glu-AdT.

necessity to use *in vitro* transcribed tRNA^{Gln} and tRNA^{Glu} variants. The crystallographic structure of *Staphylococcus aureus* GatCAB was published while this manuscript was being completed. This structure and the biochemical results obtained by gel-shift assays of the complexes formed between mutated protein and tRNA^{Gln} transcripts have shown that tRNA^{Gln} binds to the GatB subunit of the enzyme and that recognition involves the U$_1$–A$_{72}$ base pair and the D-loop of tRNA (25). Our results are compatible with the presence on the GatCAB enzyme of a unique binding site for Asp-tRNA^{Asn} and Glu-tRNA^{Gln}. This conclusion is supported by the 3D structure of *S.aureus* GatCAB which shows one active site formed by the glutaminase and transamidase catalytic sites respectively located in the GatA and GatB subunits. They are connected by a 30 Å-long tunnel which allows channelling of the ammonia from the glutaminase catalytic site to the transamidase one (25).

Finally, one can wonder how the AdTs are capable to select tRNA^{Asn} and tRNA^{Gln} out of ∼60 species of tRNA present in the organism, on the basis of a single base pair as positive element for discrimination. We therefore investigated the nature of bp 1–72 in tRNA molecules from the 84 bacterial species using AdT to form Asn-tRNA^{Asn} and/or Gln-tRNA^{Gln} and for which the sequences of the full set of tRNA encoding genes are available. The output of this analysis indicates that with the exception of a tRNA^{Thr} in *Shigella flexneri* (26), tRNA^{Asn} and tRNA^{Gln} are the only tRNA species beginning with a U$_1$–A$_{72}$ base pair (27) (data not shown). This supports the fact that specific selection of the Asp-tRNA^{Asn} and the Glu-tRNA^{Gln} amongst the other aa-tRNAs more particularly Asp-tRNA^{Asp} and Glu-tRNA^{Glu} can be achieved on the basis of the recognition of this single base pair.

CONCLUDING REMARKS

Our investigation shows that the first base pair, U$_1$–A$_{72}$, of bacterial tRNA^{Asn} acceptor arm, constitutes the unique structural element conferring to this tRNA the function of an essential cofactor in Asn biosynthesis (Figure 6A). Although our kinetic study suggests that the mode of recognition of the tRNA^{Asn} moiety of Asp-tRNA^{Asn} by bacterial AdTs might be base-specific, our results are compatible with another interpretation. Assuming that disruption of the U$_1$–A$_{72}$ pair of tRNA^{Asn} might be the key event leading to correct presentation of Asp bound to tRNA into the active site before catalysis, the importance of the U$_1$–A$_{72}$ pair would be related to the weaker hydrogen bonding stability of this base pair compared to the G$_1$–C$_{72}$ pair of tRNA^{Asp}, leading to a smaller free energy cost of base pair denaturation. In fact, it has been shown that disruption of the U$_1$–A$_{72}$ base pair of *E.coli* tRNA^{Gln}, induced by binding to GlnRS, allows discrimination of the cognate tRNA from non-cognate tRNAs by the enzyme (28,29). In *E.coli* GlnRS, a single leucine residue (Leu$_{136}$) at the tip of a β turn in the acceptor-binding domain stabilizes this disruption through hydrophobic stacking of its side chain with A$_{72}$ and G$_2$ of tRNA^{Gln}. Mutation of either Leu$_{136}$ or the residues that affect the positioning of its side chain resulted in a relaxed tRNA specificity of the enzyme (29). The 3D structure of GatCAB shows elements compatible with recognition of the U$_1$–A$_{72}$ base pair of tRNA by a mechanism
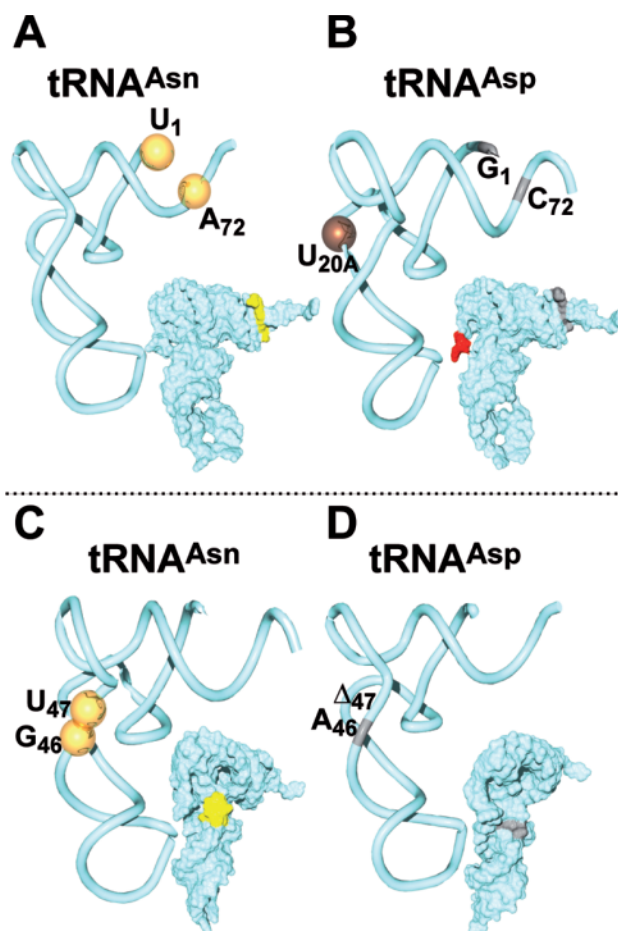

Figure 6. Localization of the elements determining (A and C) or preventing (B and D) amidation of Asp bound respectively to bacterial (**A** and **B**) and archaeal (**C** and **D**) tRNA^{Asn} and tRNA^{Asp}. The ribbon or surface representations of the 3D structures of tRNA^{Asn} and tRNA^{Asp} are compared. Since the 3D structures of bacterial and archaeal tRNA^{Asn} and of archaeal tRNA^{Asp} are not available, we used the known 3D structures of tRNA species displaying the bacterial and archaeal elements promoting or preventing transamidation to visualize the tRNA^{Asn} transamidation identity elements and the tRNA^{Asp} transamidation antideterminants. Therefore, the U$_1$–A$_{72}$ base pair conferring bacterial transamidation identity to tRNA^{Asn} (A) and the V-loop nucleotides G46 Δ47 of archaeal tRNA^{Asp} (D) are shown in the structural context of yeast tRNA^{Asp}. Similarly, nucleotides G$_{46}$ and U$_{47}$ conferring transamidation identity to archaeal tRNA^{Asn} (C) and nucleotide U$_{20A}$ preventing amidation of bacterial tRNA^{Asp} (B) are shown in the structural context of *E.coli* tRNA^{Asp}. Transamidation identity elements of tRNA^{Asn} (A and C) are represented by yellow spheres or surfaces, and their corresponding counterparts on tRNA^{Asp} (B and D) are highlighted in grey ribbon parts or surfaces. tRNA^{Asp} U$_{20A}$ anti-determinant is represented by a red sphere and surface.

resembling that of GlnRS. Indeed, the C-terminal domain of the GatB subunit, which forms the transamidation active site, contains two turn loops and a conserved leucine residue (L$_{472}$) whose deletion causes loss of tRNA-binding capacity (25). These elements are presumably good candidates for discrimination the U$_1$–A$_{72}$ base pair of tRNA^{Asn} and tRNA^{Gln} from G–C pair of tRNA^{Asp} and tRNA^{Glu}.

Discrimination between the cognate and non-cognate substrates, respectively, Asp-tRNA^{Asn} and Asp-tRNA^{Asp} by bacterial AdTs does not solely rest on the nature of the first base pair of the two tRNAs but also on the length of their D-loop

(Figure 6A and B). This suggests that these enzymes include either a domain devoted to measuring the length of the D-loop of tRNA or an active site able to sense the difference of a bulged D-loop. More surprising is the fact that quite unexpectedly, archaea and bacteria use kingdom-specific identity elements for efficient and specific transamidation of Asp-tRNA^{Asn} by their GatCAB AdTs (Figure 6). The archaeal AdTs recognize the V-region of tRNA, which constitutes a sort of hinge between the acceptor arm, i.e. the primitive tRNA and the anticodon arm which was added later in evolution to form the modern L-shaped tRNA molecule (30). In bacteria the first base pair of the acceptor arm could serve as strong transamidation identity determinant because this base pair is conserved in all tRNA^{Asn} species and it is not present in any tRNA^{Asp} molecule (Figure 6A and B). This contrasts with archaea where the first base pair is conserved in tRNA^{Asn} and tRNA^{Asp}. Therefore, discrimination between tRNA^{Asn} and tRNA^{Asp} had to be based on another part of tRNA (Figure 6C and D). Finally, based on our bioinformatics strategy that was validated by the identification of bacterial and archaeal transamidation identity elements, we predict that the same structural elements mediate specific tRNA-dependent formation of Gln in bacteria. Therefore, bacteria very likely use a unique set of transamidation identity elements for AdT-catalyzed biosynthesis of both amide amino acids.

ACKNOWLEDGEMENTS

Conflict of interest statement. None declared.

REFERENCES

1. Ibba,M., Becker,H.D., Stathopoulos,C., Tumbula,D.L. and Söll,D. (2000) The adaptor hypothesis revisited. *Trends BioChem. Sci.*, **25**, 311–316.
2. Curnow,A.W., Hong,K., Yuan,R., Kim,S., Martins,O., Winkler,W., Henkin,T.M. and Söll,D. (1997) Glu-tRNA^{Gln} amidotransferase: a novel heterotrimeric enzyme required for correct decoding of glutamine codons during translation. *Proc. Natl Acad. Sci. USA*, **94**, 11819–11826.
3. Becker,H.D. and Kern,D. (1998) *Thermus thermophilus*: a link in the evolution of the tRNA-dependent amino acid amidation pathways. *Proc. Natl Acad. Sci. USA*, **95**, 12832–12837.
4. Raczniak,G., Becker,H.D., Min,B. and Söll,D. (2001) A single amidotransferase forms asparaginyl-tRNA and glutaminyl-tRNA in *Chlamydia trachomatis*. *J. Biol. Chem.*, **276**, 45862–45867.
5. Lapointe,J., Duplain,L. and Proulx,M. (1986) A single glutamyl-tRNA synthetase aminoacylates tRNA^{Glu} and tRNA^{Gln} in *Bacillus subtilis* and efficiently misacylates *Escherichia coli* tRNA$_1^{Gln}$ *in vitro*. *J. Bacteriol.*, **165**, 88–93.
6. Stanzel,M., Schön,A. and Sprinzl,M. (1994) Discrimination against misacylated tRNA by chloroplast elongation factor Tu. Discrimination against misacylated tRNA by chloroplast elongation factor Tu. *Eur. J. Biochem.*, **219**, 435–439.
7. Tumbula,D.L., Becker,H.D., Chang,W.-Z. and Söll,D. (2000) Domain-specific recruitment of amide amino acids for protein synthesis. *Nature*, **407**, 106–110.
8. Feng,L., Sheppard,K., Tumbula-Hansen,D. and Söll,D. (2005) Gln-tRNA^{Gln} formation from Glu-tRNA^{Gln} requires cooperation of an asparaginase and a Glu-tRNAGLN kinase. *J. Biol. Chem.*, **280**, 8150–8155.
9. Schmitt,E., Panvert,M., Blanquet,S. and Mechulam,Y. (2005) Structural basis for tRNA-dependent amidotransferase function. *Structure*, **13**, 1421–1433.
10. Forchhammer,K. and Böck,A. (1991) Selenocysteine synthase from *Escherichia coli. Analysis of the reaction sequence. J. Biol. Chem.*, **266**, 6324–6328.
11. Sauerwald,A., Zhu,W., Major,T.A., Roy,H., Jahn,D., Whitman,W.B., Yates,J.R., III, Ibba,M. and Söll,D. (2005) RNA-dependent cysteine biosynthesis in archaea. *Science*, **307**, 1969–1972.
12. LaRiviere,F.J., Wolfson,A.D. and Uhlenbeck,O.C. (2001) Uniform binding of aminoacyl-tRNAs to elongation factor Tu by thermodynamic compensation. *Science*, **294**, 165–168.
13. Asahara,H. and Uhlenbeck,O.C. (2002) The tRNA specificity of *Thermus thermophilus* EF-Tu. *Proc. Natl Acad. Sci. USA*, **99**, 3499–3504.
14. Tettelin,H., Saunders,N.J., Heidelberg,J., Jeffries,A.C., Nelson,K.E., Eisen,J.A., Ketchum,K.A., Hood,D.W., Peden,J.F., Dodson,R.J. *et al.* (2000) Complete genome sequence of *Neisseria meningitidis* serogroup B strain MC58. *Science*, **287**, 1809–1815.
15. Becker,H.D., Giegé,R. and Kern,D. (1996) Identity of prokaryotic and eukaryotic tRNA^{Asp} for aminoacylation by aspartyl-tRNA synthetase from *Thermus thermophilus*. *Biochemistry*, **35**, 7447–7458.
16. Fechter,P., Rudinger,J., Giegé,R. and Théobald-Dietrich,A. (1998) Ribozyme processed tRNA transcripts with unfriendly internal promoter for T7 RNA polymerase: production and activity. *FEBS Lett.*, **436**, 99–103.
17. Curnow,A.W., Tumbula,D.L., Pelaschier,J.T., Min,B. and Söll,D. (1998) Glutamyl-tRNA(Gln) amidotransferase in *Deinococcus radiodurans* may be confined to asparagine biosynthesis. *Proc. Natl Acad. Sci. USA*, **95**, 12838–12843.
18. Becker,H.D., Min,B., Jacobi,C., Raczniak,G., Pelaschier,J., Roy,H., Klein,S., Kern,D. and Söll,D. (2000) The heterotrimeric *Thermus thermophilus* Asp-tRNA^{Asn} amidotransferase can also generate Gln-tRNA^{Gln}. *FEBS Lett.*, **476**, 140–144.
19. Fersht,A. (1985) *Enzyme Structure and Mechanism, 2nd edn.* W.H. Freeman & Co, New York.
20. Hou,Y.M. and Schimmel,P. (1988) A simple structural feature is a major determinant of the identity of a transfer RNA. *Nature*, **333**, 140–145.
21. Roy,H., Becker,H.D., Reinbolt,J. and Kern,D. (2003) When contemporary aminoacyl-tRNA synthetases invent their cognate amino acid metabolism. *Proc. Natl Acad. Sci. USA*, **100**, 9837–9842.
22. Rogers,K.C. and Söll,D. (1993) Discrimination among tRNAs intermediate in glutamate and glutamine acceptor identity. *Biochemistry*, **32**, 14210–14219.
23. Kern,D. and Lapointe,J. (1979) Glutamyl transfer ribonucleic acid synthetase of *Escherichia coli*. Effect of alteration of the 5-methylaminomethyl-2-thiouridine in the anticodon of glutamic acid transfer ribonucleic acid on the catalytic mechanism. *Biochemistry*, **18**, 5819–5826.
24. Sylvers,L.A., Rogers,K.C., Shimizu,M., Ohtsuka,E. and Söll,D. (1993) A 2-thiouridine derivative in tRNA^{Glu} is a positive determinant for

aminoacylation by *Escherichia coli* glutamyl-tRNA synthetase. *Biochemistry*, **32**, 3836–3841.

25. Nakamura,A., Yao,M., Chimnaronk,S., Sakai,N. and Tanaka,I. (2006) Ammonia channel couples glutaminase with transamidase reactions in GatCAB. *Science*, **312**, 1954–1958.

26. Sprinzl,M., Horn,C., Brown,M., Ioudovitch,A. and Steinberg,S. (1998) Compilation of tRNA sequences and sequences of tRNA genes. *Nucleic Acids Res.*, **26**, 148–153.

27. Freyhult,E., Moulton,V. and Ardell,D.H. (2006) Visualizing bacterial tRNA identity determinants and antideterminants using function logos and inverse function logos. *Nucleic Acids Res.*, **34**, 905–916.

28. Rould,M.A., Perona,J.J., Söll,D. and Steitz,T.A. (1989) Structure of *E.coli* glutaminyl-tRNA synthetase complexed with tRNA^{Gln} and ATP at 2.8 Å resolution. *Science*, **246**, 1135–1142.

29. Sherman,J.M. and Söll,D. (1996) Aminoacyl-tRNA synthetases optimize both cognate tRNA recognition and discrimination against noncognate tRNAs. *Biochemistry*, **35**, 601–607.

30. Schimmel,P. and Ribas De Pouplana,L. (1995) Transfer RNA: from minihelix to genetic code. *Cell*, **81**, 983–986.